Dear Editor,

in this document we report the modifications that we implemented in the new version of the manuscript in order to satisfy the Referees' comments.

Since we focused the analysis on the results obtained with $\Delta Z500_{HIST}$, $\Delta Z500_{SSP2}$, and $\Delta Z500_{SSP5}$ (i.e. the anomalies during HIST, SSP2, and SSP5 computed by subtracting the annual cycle of that period from the daily Z500), the manuscript has undergone major changes: some Figures were moved from the Supplement to the main manuscript (or were removed), the analysis of the results in Section 4 was modified accordingly, and Abstract and Conclusions were reviewed.

The other main changes are listed below:

- Introduction: we developed the description of blocking indexes and WTD, including pros and cons.
- Section 3: we totally reorganized section 3.1, as asked by Referee #1, and we added a new subsection (3.2) dedicated to the description of the anomalies.
  In section 3.4, we improved the descriptions of the composite and DG methods, stressing their differences. The description of these methods was also improved in the Supplement.
- Section 4: most changes in this section are resulting from the new selection of the Figures, as written above.
  In section 4.4.2, we mention a new Figure that is added in the Supplement (Fig. S6).

These changes and all the smaller corrections (like the new notation for the anomalies) are visible in the marked-up manuscript that is attached at the end of this document.
Thank you very much!

Yours faithfully,

Sara Bacer

Impact of climate change on wintertime European atmospheric blocking

Sara Bacer[1], Fatima Jomaa[1], Julien Beaumet[2], Hubert Gallée[2], Enzo Le Bouëdec[1], Martin Ménégoz[2], and Chantal Staquet[1]

[1]Univ. Grenoble Alpes, CNRS, Grenoble INP, LEGI, 38000 Grenoble, France
[2]Univ. Grenoble Alpes, CNRS, IRD, Grenoble INP, IGE, 38000 Grenoble, France

Correspondence: Sara Bacer (sara.bacer@univ-grenoble-alpes.fr)

Abstract. We study the impact of climate change on wintertime atmospheric blocking over Europe focusing on the frequency, duration, and ~~extension~~ size of blocking events. These events are identified via the weather type decomposition (WTD) methodology applied on the output of climate models of the Coupled Model Intercomparison Project phase 6 (CMIP6). Historical simulations as well as two future scenarios, SSP2-4.5 and SSP5-8.5, are considered. The models are evaluated against the reanalysis and only a subset of climate models, which better represent the blocking weather regime in the recent-past climate, is considered for the analysis. We find that frequency and duration of blocking events remain relatively stationary over the 21st century. ~~In~~ We define a methodology that relies on the WTD for the blocking event identification in order to quantify the ~~extension of~~ size of the blocking events, ~~we define a new methodology which relies on the WTD to identify blocking events.~~ and we find that the blocking size is basically unchanged in the future. We show that ~~the~~ our results are in agreement with previous studies that define blocking events with blocking indexes. ~~We find that blocking extension will increase, especially in the worst-case scenario, due to a pressure increase driven by a thermodynamical warming during blocking events rather than atmospheric circulation changes.~~

1 Introduction

Atmospheric blocking is a persistent and quasi-stationary phenomenon which highly impacts the mid-latitude circulation. By obstructing the usual westerly winds, atmospheric blocking can promote cut-off cyclones (Munoz et al., 2020) and enhance cooling in winter and warming in summer. Its long duration (from days to weeks) affects surface weather and climate and fosters regional extreme events, such as heatwaves, droughts, and severe cold weather in winter (Barriopedro et al., 2010; Woollings et al., 2018, and references therein). Blocking events are generally associated with high-pressure systems. During anticyclonic periods, solar radiation and high temperatures in summer promote ozone formation, while thermal inversions with subsidence conditions in winter promote the accumulation of particulate matter (e.g. Largeron and Staquet, 2016; Hou and Wu, 2016).

Simulating blocking is a challenging task for atmospheric models as it requires an accurate description of the topography, a fine resolution both vertically and horizontally, appropriate physical parameterizations, and a correct description of internal dynamics (Davini et al., 2017). It has been shown that general circulation models (GCMs) are able to reproduce the blocking regime and its variability, although they tend to underestimate frequency and persistence of blocking events (Dunn-Sigouin et al., 2013; Masato et al., 2013, 2014; Woollings et al., 2018; Davini and D'Andrea, 2020). Increasing model resolution can improve the blocking occurrence, as the transient eddies and orography are better described (Berckmans et al., 2013; Schiemann et al., 2017). Since atmospheric blocking is related to stratospheric variability (e.g. the stratospheric sudden warming, Davini et al., 2014), a good representation of the stratosphere can also improve blocking simulations.

The identification of blocking events ~~itself~~ in numerical simulations is complicated by the fact that blocking is determined by various dynamical mechanisms and presents different patterns. Several blocking indexes have been proposed in the literature, based on meteorological fields, usually the geopotential height at 500 hPa (e.g. Tibaldi and Molteni, 1990), or anomalies of meteorological fields (e.g. Dole and Gordon, 1983). Blocking indexes focus on different characteristics of blocking, so the choice of the index depends on the purpose of the study. Additionally, index definitions depend on various (user-dependent) parameters, like latitude band limits, latitude references, and anomaly thresholds (a review of the blocking indexes can be found in Barriopedro et al. (2010), while a recent discussion about their differences is in Pinheiro et al. (2019)). Given the variety of blocking indexes, the comparison across studies is not straightforward.

Atmospheric blocking can also be identified ~~as a weather regime (or weather type)~~ via the so-called weather type decomposition (WTD) methodology, ~~consisting in the classification of~~ which classifies the atmospheric circulation into ~~a certain number of discrete~~ discrete weather regimes (Michelangeli et al., 1995). The WTD methodology, referred to as *the WTD* hereafter for brevity, relies on a partitioning algorithm that groups data of a meteorological variable (usually geopotential height or sea level pressure) into clusters so that the variance between clusters is maximized and the variance within ~~the same~~ a given cluster is minimized. In this way, the clusters (weather regimes or weather types) are the result of a mathematical algorithm. The results of the WTD depend on certain user choices, such as the sector size, the clustering algorithm, and the initialization of this algorithm. Despite the fact that the clusters may not be well separated, WTD has proved to be very useful in the literature. In fact, WTD allows to explain most of the atmospheric variability and has largely been used to define weather regimes especially in the Northern Hemisphere (e.g. Michelangeli et al., 1995; Cassou et al., 2004; Barriopedro et al., 2006; Ullmann et al., 2014; Fabiano et al., 20 . In the European-Atlantic sector, for example, four winter weather types have been ~~recognised~~recognized: positive North Atlantic Oscillation (NAO), negative NAO, Atlantic ridge, and European blocking~~(e.g. Michelangeli et al., 1995; Cassou et al., 2004)~~ ~~.~~. The WTD has also been used to analyze weather types in relation to other quantities like temperature (e.g. Cassou et al., 2005) , precipitations (e.g. Ullmann et al., 2014), winds (e.g. Jiménez et al., 2009), and pollutants (e.g. Russo et al., 2014). In this study, the WTD is used to identify blocking events in the European-Atlantic sector.

The impact of blocking events is related to their spatio-temporal characteristics, such as occurrence, duration, and ~~extension~~size. Many studies investigated frequency and duration of blocking events in the past climate using reanalysis data (e.g. Wiedenmann et al., 2002; Barriopedro et al., 2006; Mokhov et al., 2013; Cheung et al., 2013; Drouard and Woollings, 2018; Lupo et al., 2019). Understanding the impact of climate change on atmospheric blocking is of fundamental importance to estimate future climate and extreme events, thus, blocking has also been investigated in the future in response to global warming. For example, it has been shown that the Arctic amplification, which has a strong influence on mid-latitude atmospheric circulation, modulates the frequency and the intensity of blocking events (e.g. Hassanzadeh et al., 2014). Climate models suggest that blocking frequency may decrease in the Northern Hemisphere in the future (e.g. Dunn-Sigouin and Son, 2013; Fabiano et al., 2020), and blocking activity could shift eastwards (e.g. Masato et al., 2013, 2014; Woollings et al., 2018), while there is no clear tendency for changes in blocking duration.

So far, studies have mainly focused on frequency and duration changes of future blocking events (e.g. Barriopedro et al., 2006; Patterson et al., 2019; Lupo et al., 2019). Future changes in blocking ~~extension~~ size have received less attention (Nabizadeh et al., 2019). These works determined blocking events via blocking indexes and considered one or more GCMs participating in the Coupled Model Intercomparison Project phase 5 (CMIP5). To our knowledge, only Fabiano et al. (2020) employed CMPI6 models in order to project future weather types and analyse their changes in frequency and duration.

In this study, we investigate the impact of climate change on European atmospheric blocking in terms of frequency, duration, and especially ~~extension~~size. Several GCMs of the latest model intercomparison CMIP6 are considered for this purpose under two different future scenarios (SSP2-4.5 and SSP5-8.5). In order to identify blocking events, the WTD is applied. We focus on wintertime blocking as it is more frequent, longer, and stronger than blocking in summer in the European-Atlantic sector (Barriopedro et al., 2006; Cheung et al., 2013; Lupo et al., 2019). Moreover, winter blocking events are often associated with severe particulate matter pollution episodes. We ~~introduce a new~~ define a method, referred to as *the ~~center~~ composite method*, to quantify the ~~extension~~ size of blocking events that are identified via the WTD. We compare the results obtained with this method with the results obtained for the blocking events identified via the index of Dole and Gordon (1983). Besides using GCMs of the latest CMIP phase, investigating frequency, duration, and ~~extension~~ size of blocking events that are determined via the WTD instead of blocking indexes makes this work an original study.

2 Data

Daily means of geopotential height at 500 hPa (Z500) are used for the WTD. More precisely, the WTD is applied on winter anomalies of Z500, where the winter season is defined from 1 November to 31 March (NDJFM, like in Cassou (2008), for instance). The numerical domain of Z500 covers the European-Atlantic sector whose boundaries are 80°W, 50°E, 20°N, and 80°N.

In this study, GCMs of the CMIP6 (Eyring et al., 2016) are considered. It has been shown that the weather regimes are reproduced better in CMIP6 models than in CMIP5 models, especially over the European-Atlantic sector (Fabiano et al., 2020; Davini and D'Andrea, 2020). We use historical runs to analyse blocking conditions in recent-past climate and two future projections, SSP2-4.5 and SSP5-8.5 (Riahi et al., 2017), to investigate their changes in future climate. SSP2-4.5 assumes that social, economic, and technological trends broadly follow their historical patterns and is considered as a likely scenario given the current policies. In contrast, SSP5-8.5 projects strong increments of emissions without mitigation policies; it is the worst-case scenario and is considered unlikely (Hausfather and Peters, 2020). We also use the ERA5 reanalysis of the European Centre for Medium-Range Weather Forecasts with a resolution of 31 km (Hersbach et al., 2020) to evaluate the GCM ability in reproducing the blocking weather regime.

Climate center	GCM	Acronym	Lon x Lat
Beijing Climate Center (China)	BCC-CSM2-MR	BCC	1.1°x1.1°
Canadian Centre for Climate Modelling and Analysis (Canada)	CanESM5	CanESM	2.8°x2.8°
Institute of Atmospheric Physics (China)	FGOALS-g3	FGOALS	2.0°x2.0°
National Oceanic and Atmospheric Administration (USA)	GFDL-CM4	GFDL	2.5°x2.0°
Institute of Numerical Mathematics (Russia)	INM-CM5-0	INM	2.0°x1.5°
Institut Pierre-Simon Laplace (France)	IPSL-CM6A-LR	IPSL	2.5°x1.3°
Atmospheric and Ocean Research Institute (Japan)	MIROC6	MIROC	1.4°x1.4°
Max Planck Institute for Meteorology (Germany)	MPI-ESM1-2-HR	MPI	0.9°x0.9°
Meteorological Research Institute (Japan)	MRI-ESM2-0	MRI	1.1°x1.1°

Table 1. The CMIP6-GCMs used in this study. The columns contain, respectively, the name of the research center developer of the GCM, the name of the GCM, the acronym used in this study, and the resolution of the Z500 output. All data were provided by the Mésocentre ESPRI.

The Z500 outputs considered in this study are archived in the Mésocentre ESPRI. We selected the nine CMIP6-GCMs presented in Table 1 according to the following criteria: one GCM per each climate research centre, as different versions of the same model could present model-dependent similarities (Ullmann et al., 2014); GCMs having both SSP2-4.5 and SSP5-8.5 scenarios available; GCMs with the "r1i1p1f1" run available (where "r1": initial conditions, "i1": initialization method, "p1": physical scheme, and "f1": forcing configuration), as this is the most frequently accessible simulation. The analysed periods are 30-year long: 1980-2009 (HIST hereafter) and 2070-2099 (SSP2 or SSP5 hereafter, according to the scenario).

3 Methods

3.1 Detection of the blocking weather regime

~~In this study, blocking~~ The following procedure is carried out for each GCM of Table 1 and ERA5 and for each period (HIST, SSP2, and SSP5). First, daily anomalies of Z500, noted ΔZ500, are computed as difference between the daily means of Z500 and the annual cycle (including the mean) of the 30-year period used as a climatology reference (see subsection 3.2); only the winter season (NDJFM) is retained. Second, the anomalies are weighted (multiplied) by the square root of the cosine of the latitude (Chung and Nigam, 1999) in order to account for the convergence of the meridians and to decrease the impact of high-latitude grid boxes that represent a small area of the globe (like in Cassou, 2008; Ullmann et al., 2014; Cortesi et al., 2019). Since the GCMs have different resolutions (Table 1), the anomalies are linearly interpolated onto a common grid of resolution 1°x1°.

Blocking events are identified through the application of the WTD. This weather classification has largely been used in order to infer the recurrent atmospheric features at mid-latitudes (Michelangeli et al., 1995; Philipp et al., 2016). It can be divided into two steps: dimensional reduction of the data set and clustering. Similarly to other studies (e.g. Boé and Terray, 2008; Hertig and Jacobeit, 2014; Sáenz and Durán-Quesada, 2015), we apply the Principal Component Analysis (PCA) for the first step and the k-means algorithm for the second step. ~~After the PCA ,~~ Therefore, the PCA is applied to the resulting anomalies, and the eigenvectors necessary to explain 95% of the total variance (24 eigenvectors on average) are retained to define the reduced data set. Then, k-means is applied ~~on~~ to this data set by imposing that the number of clusters (k) is equal to four, i.e. the four well-known weather types of the European-Atlantic sector (positive and negative NAO, Atlantic ridge, and European blocking), as done in Cassou (2008), Ullmann et al. (2014), and Fabiano et al. (2020)~~.~~

~~For ERA5 and each GCM of Table 1 and for each period (HIST, SSP2, and SSP5) the following procedure is followed. First, daily anomalies of Z500, noted ΔZ500, are computed as difference between the 30-year daily means of Z500 and the annual cycle of the 30-year period used as a climatology reference; only the winter season (NDJFM) is retained. Second, the anomalies are weighted (multiplied) by the square root of the cosine of the latitude (Chung and Nigam, 1999) in order to account for the convergence of the meridians and so decrease the impact of high-latitude grid boxes that represent a small area of the globe (like in Cassou, 2008; Ullmann et al., 2014; Cortesi et al., 2019). Since the GCMs have different resolutions (Table 1), the anomalies are linearly interpolated onto a common grid of resolution 1°x1°. Then, the PCA is applied to the resulting anomalies. Finally, k-means is performed~~, and each day of HIST, SSP2, and SSP5 is assigned to one of the four weather types. Only the weather regime corresponding to the European atmospheric blocking is analysed in this study. On the whole, while identifying blocking via blocking indexes implies making several choices, identifying blocking via the WTD can be considered as a standard procedure. This motivated us to apply the WTD and to explore this methodology for identifying blocking events and then studying their main characteristics (frequency, duration, size).

~~Climate change impact on blocking is quantified with respect to the historical reference period (like in Cattiaux et al., 2013; Davini and D~~
~~. This means that the HIST annual cycle is used as a climatology to compute the anomalies (Δ~~

3.2 Z500 anomalies

Climate change causes an overall increase of Z500 ~~$_{HIST}$) in all periods (HIST, SSP2, SSP5). However, in order to understand if~~ due to the warming of air masses. In order to study the changes of the spatio-temporal characteristics of blocking ~~will change~~ in the future~~because of a modified atmospheric dynamics rather than warming climate, we also compute the future anomalies by subtracting~~ , we compute the ~~corresponding SSP annual cycle~~ anomalies in all periods (HIST, SSP2, SSP5) by subtracting from Z500 the annual cycle of that period; these anomalies are noted $\Delta Z500_{HIST}$, $\Delta Z500_{SSP2}$ and $\Delta Z500_{SSP5}$. ~~Therefore, the comparison between past and future $\Delta Z500_{HIST}$ will show the impact of the total climate change signal, governed by greenhouse gases increase, global warming, and associated regional circulation changes. On the other hand,~~ Being the blocking events identified with the departure (anomaly) from the atmospheric mean state, the comparison between ~~past $\Delta Z500_{HIST}$ and future $\Delta Z500_{SSP}$ will show the blocking changes with respect to the climatology of that period; this~~ recent-past and future results will allow to quantify the dynamical climate signal ignoring the thermodynamical signal related to the anthropogenic warming. ~~Both~~ Additionally, we compute the future anomalies by subtracting from Z500 of the future periods the HIST annual cycle; these anomalies are noted $\Delta Z500_{\cancel{HIST}SSP2\text{-}HIST}$ and $\Delta Z500_{\cancel{SSP}SSP5\text{-}HIST}$~~undergo the same analysis process; since the final aim of this work is to investigate the net climate change~~ . In this case, the comparison between recent-past and future anomalies will show the net impact on blocking ~~, the results obtained with ΔZ500$_{SSP}$ that are similar to the ΔZ500$_{HIST}$ results are included in the supplementary material.~~ of the total climate change signal, governed by greenhouse gases increase, global warming, and associated regional circulation changes.

3.3 Definition of blocking events

Consecutive days that belong to the blocking weather type can form a blocking event. The blocking events considered in this study satisfy the following conditions: they must be longer than five days (like in Barriopedro et al., 2006; Matsueda et al., 2009; Mokhov et al., 2013) and separated by at least two non-blocking days. A single non-blocking day (“hole”) is assumed to represent a failure of k-means in that day, like in Matsueda et al. (2009). Therefore, the k-means result is processed in such a way that 1) two blocking events equal to/longer than two days separated by a hole form one blocking event ~~; one blocking day and~~ and 2) one blocking event equal to/longer than three days and one blocking day separated by a hole (and then vice versa) form one blocking event.

We clarify here the meaning of some specific terms. We call *centroids* the four centres of mass defined by the k-means algorithm in the reduced space, i.e. the space whose coordinates are the eigenvectors. Weather regime (or weather type) refers to the centroid transformed into the original latitude-longitude coordinate space. From now on, we call *blocking days* those days which belong to a blocking event. Finally, we refer to the temporal mean of ΔZ500 over the blocking days of a blocking event as the *composite* of that event.

3.4 Computation of blocking area

We quantify the ~~extension~~ size of a blocking event by its area. Two distinct methods are used to compute the blocking area: the so-called ~~center~~ composite method, introduced in this study, and the *DG method*, used by Nabizadeh et al. (2019).

~~Center~~ Composite method. We introduce this method to compute the area of the composites of the blocking events inferred from the WTD. The ~~center~~ composite method starts from the detection of the center of each ~~blocking event~~composite. In this study, we define as *center* of the European atmospheric blocking the location of the maximum positive anomaly of the composite between 30°W and 50°E (similarly to Barriopedro et al., 2006), in order to discard blocking ~~events~~ with positive anomaly on the westernmost part of the sector. The ~~extension of the blocking event~~ blocking size is quantified by the area enclosed within the contour line equal to a certain threshold. In order to get ~~non vanishing~~ non-zero areas, we define a threshold of ΔZ500 that must be lower than the minimum value among the centers over all periods and all GCMs. In this study, the threshold is 75 m considering ΔZ500$_{HIST}$, ΔZ500$_{SSP2}$, and ΔZ500$_{SSP5}$ and 100 m considering the ΔZ500 with respect to the recent-past climatology (i.e. ΔZ500$_{SSP2\text{-}HIST}$ and ΔZ500$_{SSP5\text{-}HIST}$). For the purpose of this study, which requires a comparison between past and future results among several GCMs, we keep the thresholds constant for the entire analysis. Technical details about the ~~center~~ composite method are reported in the Supplement.

DG method. This method follows the work of Nabizadeh et al. (2019), who determined the ~~extension~~ size of the atmospheric blocking events identified with the index of Dole and Gordon (1983) (DG index hereafter). ~~First, they~~ Thus, we also compute the daily DG index for each grid box of the domain ~~. Second, they~~ and identify as blocking events those grid boxes where the DG index is higher than 1.5 for at least five consecutive days. We will refer to these days as *DG-blocking days* and to the blocking events as *DG-blocking events*. ~~Then~~The DG method consists in computing, for each DG-blocking day, ~~they compute~~ the area enclosed by the contour line where the DG index is equal to one~~(~~, i.e. the contour line equal to a certain threshold of $\Delta Z500$~~). Finally~~: 112 m for $\Delta Z500_{\mathrm{HIST}}$, $\Delta Z500_{\mathrm{SSP2}}$, and $\Delta Z500_{\mathrm{SSP5}}$ and 116 m for the $\Delta Z500$ with respect to the recent-past climatology. Then, daily areas are averaged along the event duration to get the area of the DG-blocking event (more details about the DG method are in the Supplement). In the present paper, the DG-blocking days ~~will be~~ are identified within the blocking events inferred from the WTD (and ~~therefore~~ not during the entire winter, as considered by Dole and Gordon (1983)).

~~The blocking areas presented in subsection 4.4 will be computed via both the center method~~ Therefore, these methods compute the area of blocking events that are identified via two different approaches: the WTD and the DG ~~method. As previously mentioned, a certain threshold is defined in both methods to delimit the blocking extension. For the purpose of this study, which requires a comparison between past and future results among several GCMs, we keep the thresholds constant for the entire analysis~~index. Although the algorithm to compute the blocking area within a certain contour line is the same, it is applied on blocking composites in the composite method and on daily $\Delta Z500$ in the DG method. Another difference between these two methods is the definition of the $\Delta Z500$ values of the contour lines (i.e. the thresholds).

4 Results and Discussion

4.1 Evaluation of the GCMs

Before analysing the impact of climate change on European atmospheric blocking events, the ability of the GCMs (Table 1) in reproducing ~~the blocking weather regime~~ atmospheric blocking is evaluated with respect to the reanalysis with a Taylor diagram (Figure 1). This diagram compares the blocking composites of each GCM during HIST with the ERA5 ~~composites~~composite. The deviation is quantified in terms of pattern correlation (R), standard deviation (σ), and root-mean-square difference (RMSD). All GCMs are able to represent blocking variability (i.e. σ) quite close to the variability obtained with the reanalysis ($\sigma_{ERA5} \cong 61$ m). More precisely, the variability of all GCMs is within the range $\sigma_{ERA5} \pm 6$ m, apart from INM and IPSL. Six models (MPI, BCC, MRI, GFDL, INM, and FGOALS) show a high correlation ($R \geq 0.79$) with ERA5, while three models (CanESM, MIROC, and IPSL) present a lower correlation ($R < 0.6$) and a high RMSD. Hertig and Jacobeit (2014) also found that historical runs of CanESM cannot well reproduce the blocking pattern, getting a correlation with reanalysis lower than 0.4. In this study, CanESM is the GCM with the coarsest resolution (Table 1), and it has been shown that a low resolution hinders a good description of the atmospheric variability patterns (Berckmans et al., 2013).

This analysis points out that MIROC, ~~IPSL, and CanESM~~ CanESM, and IPSL are less accurate in capturing the blocking pattern in recent-past climate (as also observable in Figure ~~??~~2, e-f-g), and we expect these models to be less reliable in future projections of blocking. Previous studies (e.g. Chhin and Yoden, 2018; Mokhov and Timazhev, 2019; Khan et al., 2020) suggest to use a subset of GCMs selected according to their ability in simulating the quantity of interest (atmospheric blocking in this study) in the past in order to reduce the uncertainties associated to the future projections of that quantity. Therefore, we exclude MIROC, ~~IPSL, and CanESM~~ CanESM, and IPSL from the next analysis and focus on the results obtained by the other

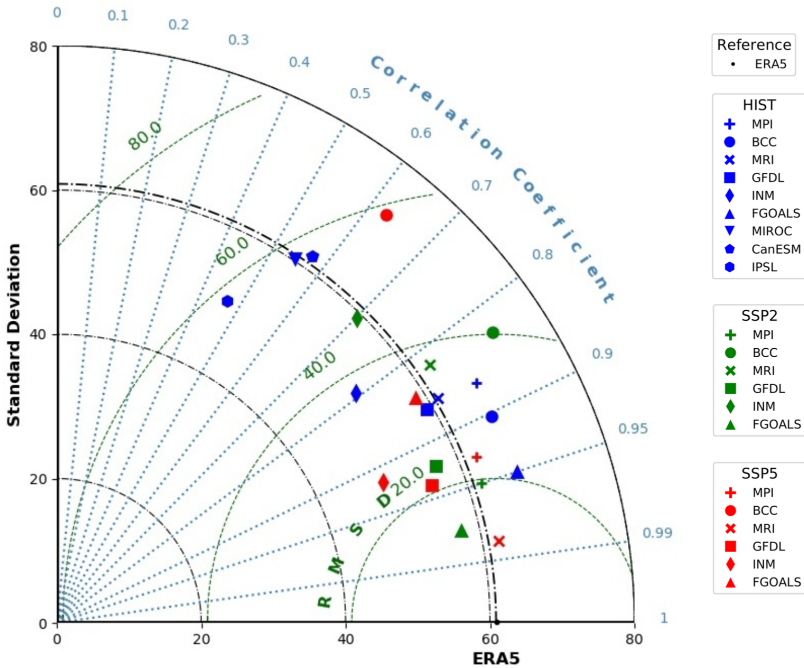

Figure 1. Taylor diagram for the mean composites over all blocking events for ERA5 and all GCMs for the winter HIST period (1980-2009). The diagram allows to quantify standard deviation (black), correlation coefficient (light blue), and root-mean-square difference (green) between the mean GCM composites and the mean ERA5 composite. SSP2 and SSP5 results are obtained with $\Delta Z500_{\cancel{\mathrm{HIST}}\,\mathrm{SSP2}}$ and $\Delta Z500_{\mathrm{SSP5}}$, respectively.

six GCMs: MPI, BCC, MRI, GFDL, INM, and FGOALS. In the same Taylor diagram~~(Figure 1)~~, blocking projected for future climates (both SPP2 and SSP5) by these six GCMs is also shown. Overall, correlation coefficients, standard deviations, and RMSDs vary in a non-systematic way, so we do not find any regularity in the reproducibility of future blocking by the GCMs.

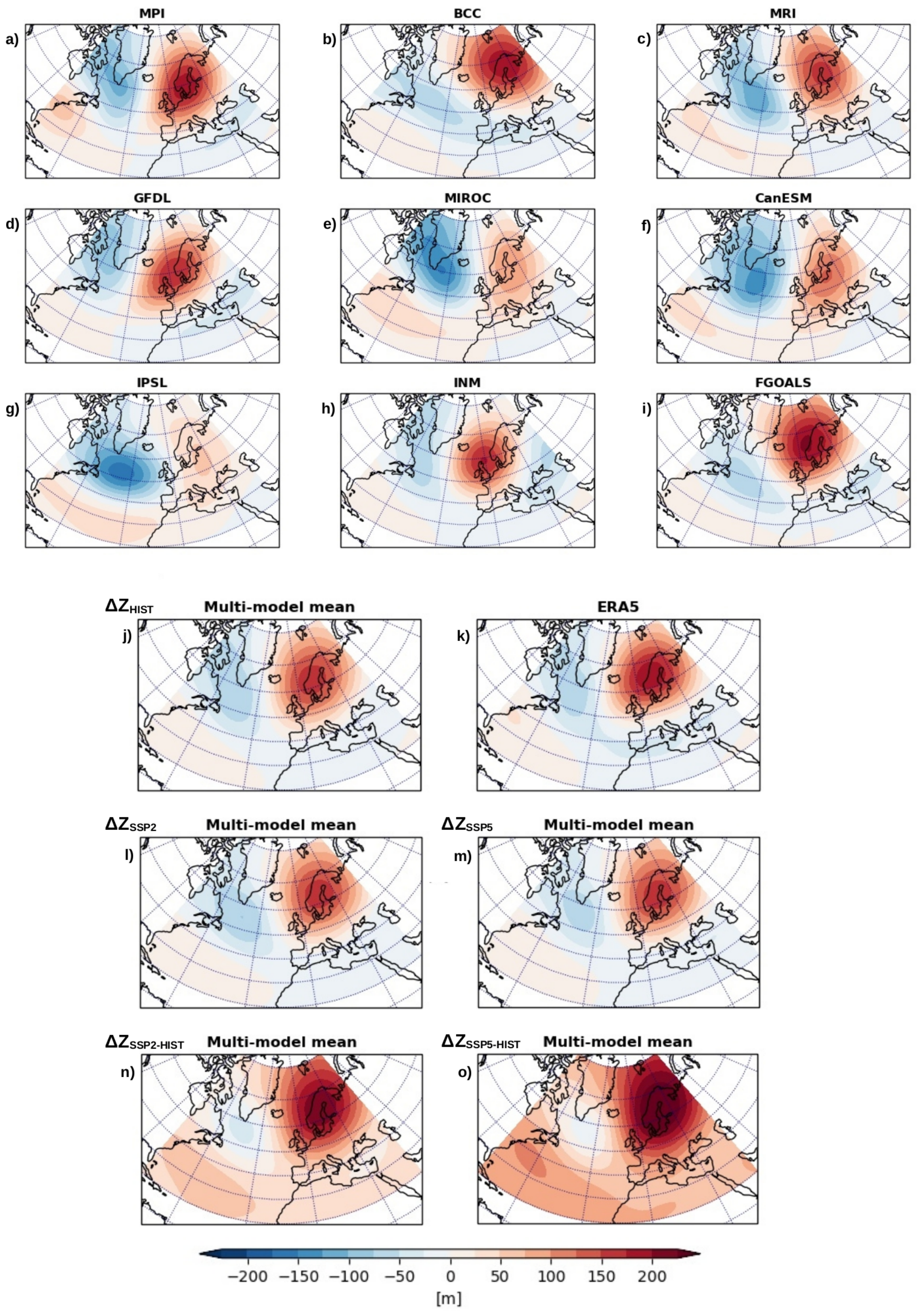

Figure 2. ~~$\Delta Z500_{HIST}$~~ Blocking composites averaged over all blocking events for all GCMs (a-i) and ERA5 (k) during the winter HIST period (1980-2009)~~; in the last row, the~~. The multi-model ~~mean is~~ means are computed over all blocking events of the six selected GCMs for the HIST period (1980-2009) using $\Delta Z500_{HIST}$ (j) and for the future period (2070-2099) using $\Delta Z500_{SSP2}$ (l), $\Delta Z500_{SSP5}$ (m), $\Delta Z500_{SSP2\text{-}HIST}$ (n), and $\Delta Z500_{SSP5\text{-}HIST}$ (o).

~~ΔZ500$_{HIST}$ composites averaged over all blocking events for the six selected GCMs during the winter SSP2 period (2070-2099); in the last row, the multi-model mean is computed over all blocking events of the six selected GCMs.~~

The spatial patterns of blocking during recent-past climate are shown in Figure ~~??~~2 (a-i). All GCMs are considered during HIST, and the dissimilarity of CanESM, MIROC, and IPSL with respect to ERA5 (Figure 2, k) is evident. According to the reanalysis, the European blocking is centred over the Scandinavian peninsula and extends over northern Europe. Blocking occurrence is about 27% (Table S1 in the Supplement) in accordance with previous studies that considered, for example, NCEP/NCAR reanalysis (27%, Cassou, 2008) and ERA-interim reanalysis (26%, Ullmann et al., 2014). MPI, BCC, and MRI reproduce an occurrence similar to ERA5, while GFDL, INM, and FGOALS simulate less frequent blocking with an occurrence of about 23%. We observe that the first three models have the highest resolution (see Table 1), so we also find that the underestimation of atmospheric blocking occurrence is reduced in ~~high~~ higher resolution GCMs. We compute the multi-model (MM) mean as the average of the composites over all blocking events of the six selected GCMs. The spatial pattern of the MM mean ~~in HIST~~ during HIST (Figure 2, j) is very close to the ERA5 blocking, as also demonstrated by the statistics: $R \cong 0.98$, RMSD$\cong 13\ \mathrm{m}$, and $\sigma_{MM} \cong 56\ \mathrm{m}$.

In future climate (~~SSP2 in Figure ?? and SSP5 in Figure S2), the most evident change in blocking obtained with ΔZ500$_{HIST}$ is the extension, which gets wider in SSP2 and especially in SSP5. Moreover, the centers of future blocking are characterised by higher values of anomalies in comparison with ERA5; also in this case, the changes are emphasised in SSP5. On the contrary, analysing ΔZ500$_{SSP}$ we find that the spatial patterns of the future blocking composites (Figure S3)~~ Figure 2, l-m), the spatial characteristics of the blocking composites are very similar to the ~~results obtained for~~ ones of the HIST period (~~all these results will be confirmed in subsections 4.3 and 4.4). ~~The strong differences in blocking extension and intensity between~~ Considering the ΔZ500$_{\cancel{HIST}\,SSP2\text{-}HIST}$ and ΔZ500$_{\cancel{SSP}\,SSP5\text{-}HIST}$ results ~~indicate that future blocking changes are mainly due to thermodynamical than dynamical changes.~~(Figure 2, n-o), blocking events get wider in SSP2 and especially in SSP5 and their centers are characterised by higher values. (The blocking composites computed for each GCM in the future are in Figures S2 and S3 in the Supplement.) Thus, we find that atmospheric blocking presents a dynamical component whose pattern is relatively stationary over the 21st century and a thermodynamical component that~~evolves~~ , as expected, is broadly driven by the overall warming of air masses in relation with the anthropogenic signal.

4.2 Frequency and duration of blocking events

~~Number of blocking days (*left*) and blocking events (*center*) averaged over all winters of the 30-year periods, and mean duration (in days) of blocking events occurred in 30 winters (*right*) for recent-past climate and future scenarios (SSP2-4.5 and SSP5-8.5) considering ΔZ500$_{HIST}$. The black dashed line is the ERA5 mean. (The values are taken from Table S2.)~~

Blocking events are identified for each GCM following the definition in subsection 3.3. The number of blocking days and blocking events per winter averaged over all winters of the 30-year periods and the duration of blocking events averaged over these periods are graphically represented in Figure 3 to facilitate the comparison of the HIST results against ~~reanalysis and~~ the future (SSP2 and SSP5) results. We find that, during recent-past conditions, the MM mean number of blocking days per winter is about 30 and the MM mean number of events per winter is about ~~3 (Figure 3 and Table S2).~~ 3. Our results are slightly lower than the findings of Mokhov et al. (2014), 35.8 days and 4.7 events, who detected blocking events in an Euro-Atlantic sector using a Z500-based blocking index applied on one GCM (IPSL). The MM mean of blocking duration is 9.9 ± 0.9 days and is close to the mean duration of blocking events of 10.2 ± 5.3 days obtained with the reanalysis. These results are in agreement with mean blocking durations found in the literature, e.g. 10.5 days for winter blocking in the European-Atlantic sector by Lupo et al. (2019), using reanalysis (NCEP/NCAR) of Z500, and 7.6 days by Mokhov et al. (2014). In summary, the mean temporal characteristics of blocking events are well reproduced by the GCMs: the MM means of number of blocking days and duration during HIST are close to the results obtained with the reanalysis, although most of the models tend to underestimate these quantities.

When analysing the impact of climate change, no significant impact is found on blocking frequency and duration. With respect to the HIST results, MPI, BCC, and MRI simulate less frequent blocking events in both future scenarios, while the other GCMs present a higher blocking frequency (Figure 3). However, the uncertainty of the results is large (Table S2), so the differences between the periods are not statistically significant. Additionally, results for SSP2-4.5 and SSP5-8.5 are not in agreement among the various models (sometimes estimates are higher in SSP2 and sometimes in SSP5). ~~Nevertheless, we observe that the MM means of the mean number of blocking days per winter and the mean duration of blocking events will decrease by about one day and half a day, respectively. Interestingly, the results obtained with $\Delta Z500_{HIST}$ are very similar to the results obtained with $\Delta Z500_{SSP}$ (Figure S4). This suggests that the tendency of blocking frequency to decrease in the future is due to changes of the atmospheric dynamics under the SSP2-4.5 and SSP5-8.5 scenarios. However, the uncertainty of the results is very large (Table S2), so the differences between the periods are not statistically significant.~~ Actually, a clear long-term change in blocking frequency in the past has not emerged so far (Barnes et al., 2014; Woollings et al., 2018), and there is no general consensus on the tendency of blocking frequency in future climate (Woollings et al., 2018). For example, ~~and~~ Matsueda and Endo (2017) found a significant decrease in blocking frequency in the European-Atlantic sector involving all durations of blocking events simulated with six CMIP5-GCMs, Mokhov et al. (2014) found a general increase in the blocking frequency, while Masato et al. (2014) found that European blocking frequency remains unchanged using four CMIP5-GCMs.

The analysis of the occurrence of blocking events as a function of duration also indicates that the GCM projections agree well with the reanalysis (Figure 4 and Figure~~S5~~ S4). Occurrence of blocking events decreases exponentially with duration, consistent with the findings of Wiedenmann et al. (2002); Barriopedro et al. (2006); Matsueda et al. (2009); Dunn-Sigouin and Son (2013); Mokhov et al. (2014). The distributions of all periods show long tails up to 30 days, but some isolated events can be even longer. In future climate~~(both SSP2 and SSP5)~~, we find that the occurrence of short (5-8 days) blocking events ~~increases~~slightly increases under the SSP5-8.5 scenario, while the occurrence of long (more than 10 days) events tends to decrease, as indicated by the mean ~~lifetimes~~ lifetime (τ) of the exponential ~~fits, which are lower for SSP2 and~~ fit, which is lower for SSP5 ($\tau \approx$9 days) than for SSP2 and HIST ($\tau \approx$10 days). ~~It must be noted that these results, obtained with $\Delta Z500_{HIST}$, are very close to the $\Delta Z500_{SSP}$ results (Figure S6).~~

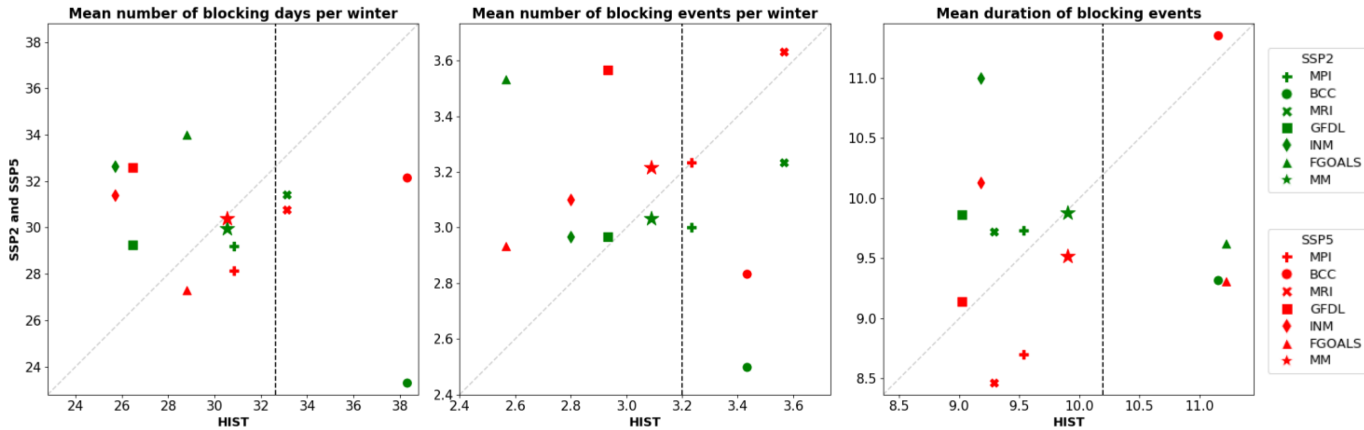

Figure 3. Number of blocking days (*left*) and blocking events (*center*) averaged over all winters of the 30-year periods, and mean duration (in days) of blocking events occurred in 30 winters (*right*) for recent-past climate and future scenarios (SSP2-4.5 and SSP5-8.5) considering $\Delta Z500_{HIST}$ (x-axis) and $\Delta Z500_{SSP2}$ and $\Delta Z500_{SSP5}$ (y-axis). The black dashed line is the ERA5 mean. (The values are taken from Table S2.)

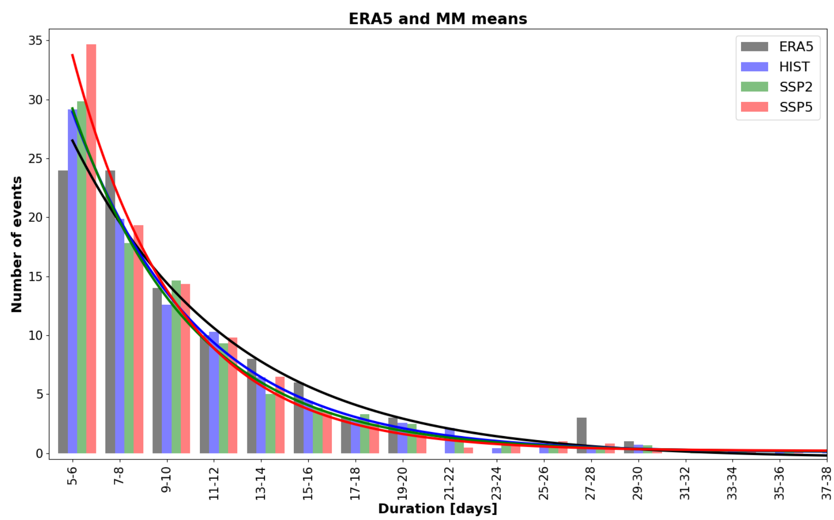

Figure 4. Occurrence of blocking events as a function of duration for ERA5 and MM means during HIST, SSP2, and SSP5, considering $\Delta Z500_{HIST}$, $\Delta Z500_{SSP2}$, and $\Delta Z500_{SSP5}$. Exponential fits are drawn for ERA5 and MM means.

4.3 Centers of blocking events

We now analyse the blocking centers (as defined in subsection 3.4) of the composites of blocking events ~~. We study the impact of climate change on the blocking centers~~ in terms of their location and intensity, i.e. the value of $\Delta Z500$ at that location. The geographical distribution of the center locations averaged over all blocking events of a given 30-year period is shown in Figure 5. The ERA5-center is located over Sweden. The GCM-centers during HIST are over and close to the Scandinavian

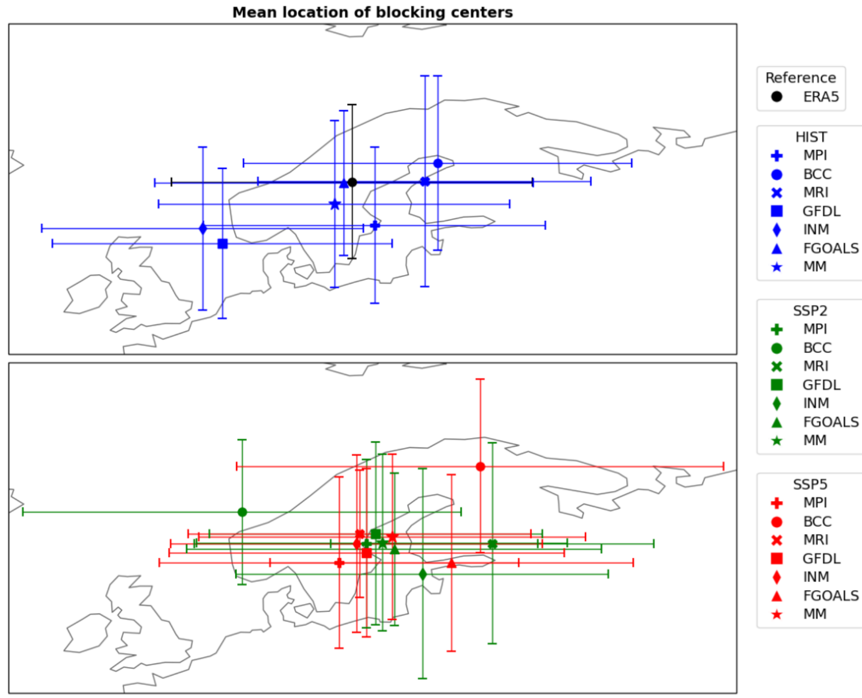

Figure 5. Locations of the blocking composite centers averaged over all blocking events for ERA5 and the GCMs during HIST considering $\Delta Z500_{HIST}$ (*top*) and during SSP2 and SSP5 considering $\Delta Z500_{SSP2}$ and $\Delta Z500_{SSP5}$ (*bottom*). The error bars indicate the standard deviations of latitudinal and longitudinal coordinates of the blocking centers.

peninsula. In the future, we observe a general eastward shift of the center locations~~using $\Delta Z500_{HIST}$~~. In particular, four out of six models during SSP2 and ~~all models during~~ SSP5 show blocking centers that are eastward with respect to the centers in HIST. The SSP2- and SSP5-MM means of the center locations are located about ~~6~~4° and ~~9~~5° eastward to the HIST-MM mean, respectively. An eastward shift of European blocking would lead to an increase of blocking over Western Russia (Dunn-Sigouin and Son, 2013). More uncertain is the meridional shift of the centers in the future~~(three GCMs, GFDL, MPI, and INM, show a northward shift). Similar considerations are also valid for $\Delta Z500_{SSP}$ (Figure S7), although the eastward shift tendency is even less evident (between 4° and 5° in both future scenarios)~~. An eastward and northeastward shift of European blocking was also found by Masato et al. (2013, 2014) and Sillmann and Croci-Maspoli (2009), respectively. However, it must be stressed that there is a large variability associated to the blocking center locations on both meridional and zonal directions (as attested by the error bars in Figure 5), and the shift of the centers is not significant.

The MM mean of the blocking center intensities during HIST is 248 ± 18 m, very close to the ERA5-intensity, 251 ± 48 m (Table S3). The minimum intensity is simulated by INM, 219 ± 50 m, the maximum one by MPI, ~~274 ± 61 m.~~ 273 ± 61 m. Under the SSP2-4.5 and SSP5-8.5 scenarios, the ~~MM means of the intensities increase with respect to the~~ center intensities are very similar, on average, to the intensities of the blocking events in recent-past conditions ~~in both future scenarios, especially~~

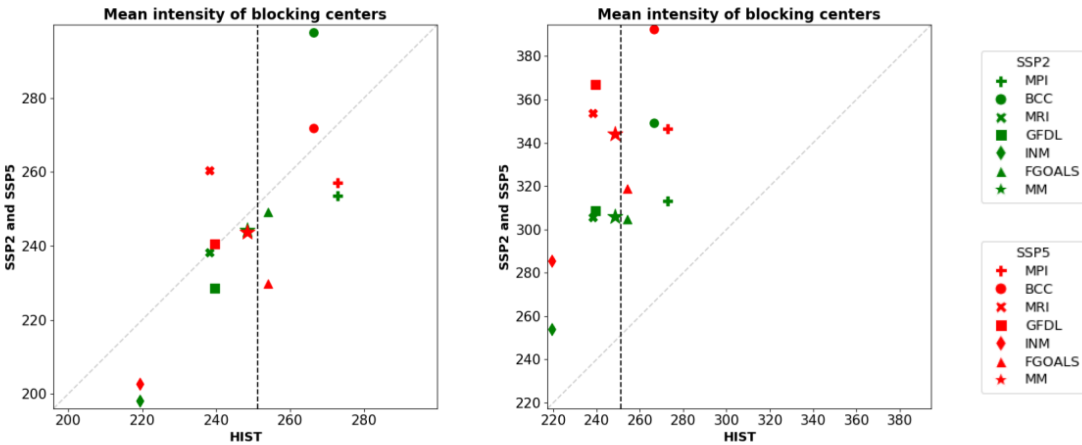

Figure 6. Intensities (in m) of the blocking composite centers averaged over all blocking events during HIST, SSP2, and SSP5 considering $\Delta Z500_{HIST}$ on the x-axis and $\Delta Z500_{SSP2}$ and $\Delta Z500_{SSP5}$ (*left*) and $\Delta Z500$~~$_{SSP}$~~ $_{SSP2\text{-}HIST}$ and $\Delta Z500_{SSP5\text{-}HIST}$ (*right*) on the y-axis. The black dashed line is the ERA5 mean. (The values are taken from Table S3.)

~~in the worst-case scenario~~ (Figure 6, left). ~~In particular, they increase up to 306 m in SSP2~~ Also the variability of the centers, in terms of standard deviations and ~~344 m in SSP5. Although the variability increases as well (see the standard deviations in~~ minimum-maximum intervals of the intensities (Table S3), ~~the intensity increments (of~~ do not change, implying that the future blocking intensities will be not affected by atmospheric dynamical changes. Additionally, we observe that differences between SSP2 ~~versus HIST~~ and SSP5 ~~versus HIST) are significant. Mokhov et al. (2014) also found a tendency for an increasing blocking intensity in the European-Atlantic sector in the 21st century, in winter, by analysing similar scenarios(RCP2.6~~ periods are smaller than inter-model differences. On the contrary, the center intensities of the future blocking events identified using $\Delta Z500_{SSP2\text{-}HIST}$ and ~~RCP8.5). Moreover, we observe that the minimum intensities of all GCMs are higher~~ $\Delta Z500_{SSP5\text{-}HIST}$ (i.e. the anomalies obtained using the recent-past climatology as reference) increase with respect to the recent-past conditions in both future scenarios, especially in the worst-case scenario (Figure 6, right). In particular, their MM means increase up to 306 m in SSP2 ~~than in HIST, and even higher~~ and 344 m in SSP5~~; this is valid also for the maximum intensities of almost all models (Table S3).~~. The ~~significant increase~~ increments of the center intensities (i.e. of the geopotential height) ~~found by all GCMs in the future considering $\Delta Z500_{HIST}$ is~~ in this case are mainly explained by the general warming related to the anthropogenic greenhouse gases emissions occurring under the considered scenarios. ~~On the contrary, the center intensities of the future blocking events identified using $\Delta Z500_{SSP}$ are very similar, on average, to the intensities of the blocking events in recent-past conditions (Figure 6, right and Table S3), implying that the future changes of blocking intensity will be not affected by atmospheric dynamical changes.~~

~~Locations of the blocking composite centers averaged over all blocking events for ERA5 and the GCMs during HIST (*top*), SSP2, and SSP5 (*bottom*) considering $\Delta Z500_{HIST}$. The error bars indicate the standard deviations of latitudinal and longitudinal coordinates of the blocking centers.~~

4.4 ~~Extension~~ Size of blocking events

4.4.1 ~~Center~~ Composite method

Blocking area is computed for each composite of blocking event by using the ~~center~~ composite method described in subsection 3.4. This method takes into account events whose center is between 30°W and 50°E to focus on European blocking, ~~nevertheless,~~ although some events can extend westwards in the European-Atlantic sector. This is due to the fact that the events ~~have been~~ are identified via a partitioning algorithm (k-means) and not via blocking indexes designed for geopotential fields that are typical during atmospheric blocking. We could verify that, on average, only four events per GCM (i.e. $\sim 4\%$) are of this type during HIST~~. This effect is more frequent considering $\Delta Z500_{HIST}$ in the future, especially in SSP5, as the threshold more often allows for the detection of "stretched" shapes. We~~ ; we preferred not to disregard them in order not to introduce any subjectivity into the analysis, and the results are considered as an overestimation of the blocking ~~extension, especially in the future~~size.

The MM mean ~~extension~~ size in HIST is ~~$7.0 \cdot 10^6$ km^2~~ $9.1 \cdot 10^6$ km^2, very close ~~(1.4% larger)~~ to the value obtained for ERA5 (Table S4). ~~This extension is nearly twice (1.7) and three times (2.7) larger for~~ As expected from Figure 2, the future blocking size is comparable to the recent-past blocking size. Actually, the MM mean size decreases by $0.3 \cdot 10^6$ km^2 (i.e. about 3%) during SSP2 and SSP5~~. As expected from Figures **??**, **??**, and S2, we find~~ , although not in a statistically significant way. Different results are obtained for the future blocking size computed with respect to the recent-past climatology (as anticipated in Figure 2, n-o). In this case, there is a clear tendency of blocking ~~extension~~ size to increase in the future~~, especially in the worst-case future scenario (in agreement with Nabizadeh et al., 2019). The fact that positive anomalies get larger in the future~~ ; the size is nearly twice (1.7) and three times (2.7) larger during SSP2 and SSP5, respectively. This is mainly due to the global warming projected with the SSP2-4.5 and SSP5-8.5 scenarios, as already noted in subsection 4.1. ~~Different results are obtained for the future blocking extensions computed with $\Delta Z500_{SSP}$. In this case, the MM mean extensions in SSP2 and in SSP5 are similar (Table S4). Moreover, they are comparable to the blocking area in recent-past conditions (as anticipated in Figure S3).~~

We further analyse the blocking ~~extension~~ size results in relation to the center intensity. We find a linear relation between ~~extension~~ size of blocking events and intensity of blocking centers ~~considering both $\Delta Z500_{HIST}$ and $\Delta Z500_{SSP}$~~ (Figure 7, left). The correlation is significant and higher than ~~0.8 in the~~ 0.7 during HIST and SSP2~~cases~~. The linear relation is in agreement with Barriopedro et al. (2010). Again, our results are in line with previous studies that followed a different approach for the blocking detection, based on the use of blocking indexes instead of the WTD.

~~We observe that the blocking extension estimated for the GFDL model during SSP5 using $\Delta Z500_{HIST}$ is much higher than the other GCMs (Figure 7 and Table S4). The reason is that the blocking events in GFDL are characterised , on average, not only by a large positive anomaly over North Europe, but also by an evident positive anomaly over the Atlantic Ocean close to the US coast (Figure S2). As a consequence, the shape of what is considered blocking extension in the center method is often elongated until North America (not shown). Since this type of shape cannot be attributed to the European blocking, the previous analysis has been performed also neglecting the GFDL model. In this case, the linear regression between blocking extension and center intensity during~~ Figure 8 (left) and Figure S5 show that blocking size is characterised by a normal distribution (e.g. Whiteman, 1982; Barriopedro et al., 2006). This is valid in all periods. In particular, the MM means of blocking area during SSP2 and SSP5 ~~is higher than 0.8 as well (Figure 7, left), thus, the GFDL results for SSP5-8.5 have not been considered in the next analysis with $\Delta Z500_{HIST}$.~~

~~Figure 8 shows that blocking extension is characterised by a normal distribution (e.g. Whiteman, 1982; Barriopedro et al., 2006). The similarity between the distribution obtained with reanalysis and historical GCM data is noteworthy (Figure 8 and Figure S8). The blocking extensions obtained with future~~ are very similar and close to the MM mean of the past blocking area. Different results are obtained for future blocking size computed with $\Delta Z500_{\cancel{HIST}SSP2\text{-}HIST}$ ~~can be only roughly approximated by a gaussian low, especially in SSP5~~ and $\Delta Z500_{SSP5\text{-}HIST}$ (Figure 8, ~~left). The results obtained in this caseshow that climate change will impact the distribution of future blocking area:~~ right). In this case, more blocking events with larger ~~extension~~ size will occur, as proved by the shift of the distribution towards higher values and its increasing width~~(although we remind that blocking area~~. Moreover, we notice that the blocking size in the future ~~is likely overestimated in this study). Different results are obtained for future blocking extensions computed with $\Delta Z500_{SSP}$ (Figure 8, right). In this case, the MM means of blocking area during SSP2 and~~ can be only roughly approximated by a gaussian low, especially in SSP5~~are very similar and close to the past blocking extension, as already inferred with Figure S3~~. It must be ~~specified that , since some values of center intensities are smaller than~~ reminded that the threshold chosen for ~~the~~ $\Delta Z500_{HIST}$~~case (100 m)~~, $\Delta Z500_{SSP2}$, and $\Delta Z500_{SSP5}$ (75 m) is lower than the threshold used ~~for the center method in the~~ with $\Delta Z500$ ~~$_{SSP}$ case is different (75 mfor all periods, HIST, SSP2, and SSP5, see the Supplement for more details~~with respect to the recent-past climatology (100 m, see subsection 3.4).

4.4.2 Comparison with the DG method

In order to check the reliability of the ~~center~~ composite method in estimating the area of blocking events, we compute that area by another approach relying on the DG index to identify blocking events, as done by Nabizadeh et al. (2019). As indicated in subsection 3.4, the latter events will be denoted DG-blocking events; for clarity, in this section, the blocking events identified by the WTD will be denoted WTD-blocking events.

~~As explained in subsection 3.4 and in the Supplement, we~~ We apply the DG method to compute the area of those DG-blocking days that belong to the WTD-blocking events (see subsection 3.4). Despite the number of these DG-blocking days may not match with the duration of the respective WTD-blocking events, we find that ~~it agrees well with the duration of the WTD-blocking events. Such agreement improves from HIST to SSP2 and to SSP5 considering $\Delta Z500_{HIST}$. This is due to the fact that the positive anomalies get wider in SSP2 and even more in SSP5, the DG index is higher than 1.5 more often, and thus the DG-blocking events embrace or well overlap the WTD-blocking events of the SSP2 and SSP5 periods~~the two quantities generally agree (Figure S6).

The blocking areas resulted from the ~~center~~ composite method and the DG method are compared in Figure ~~??~~7 (right). These areas are linearly correlated with statistical significance in all periods, the slopes of the linear regression being ~~larger than 0.79 with $\Delta Z500_{HIST}$ and 0.68 with $\Delta Z500_{SSP}$. We can conclude that the extension~~ around 0.70 or larger (in SSP5). Therefore, the size of the blocking events identified via the WTD is in agreement with the ~~extension~~ size of the blocking events identified via the DG index.

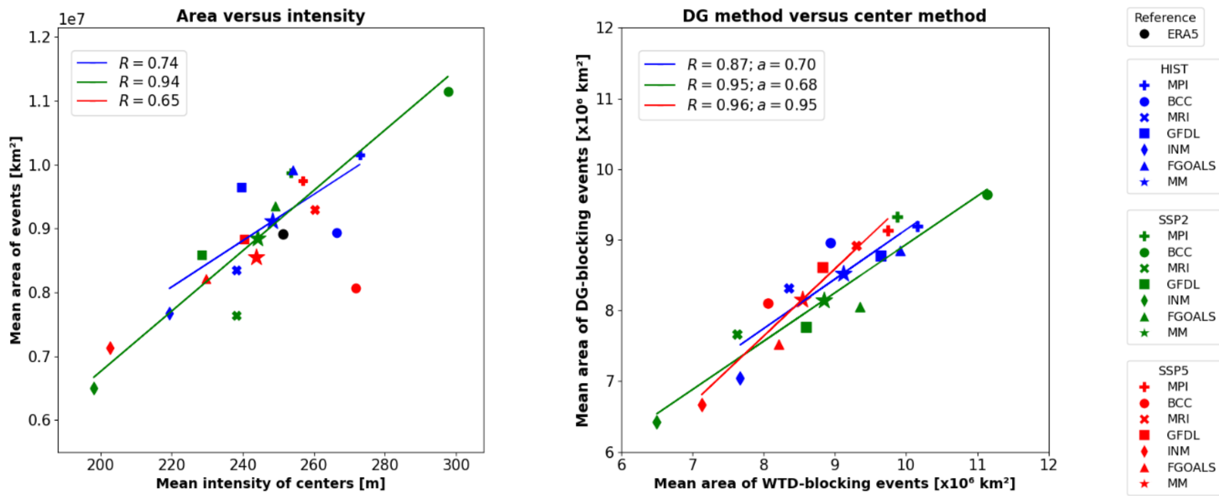

Figure 7. (*Left*) Mean area versus mean center intensity of blocking events computed for ERA5 and the GCMs during HIST, SSP2, and SSP5~~considering~~ ~~$\Delta Z500_{HIST}$~~ ~~*(left)* and~~ ~~$\Delta Z500_{SSP}$~~ ~~*(right)*~~. (*Right*) Mean area of blocking events computed with the DG method versus mean area of blocking events computed with the composite method. R is the correlation; ~~R^*~~ a is the ~~correlation excluding GFDL~~slope of the linear regression; regression lines (found by the least-squares fit~~excluding GFDL in SSP5 in *(left)*~~) are drawn when the correlation is statistically significant (at the 90% confidence level). Both plots show the results for $\Delta Z500_{HIST}$, $\Delta Z500_{SSP2}$, and $\Delta Z500_{SSP5}$.

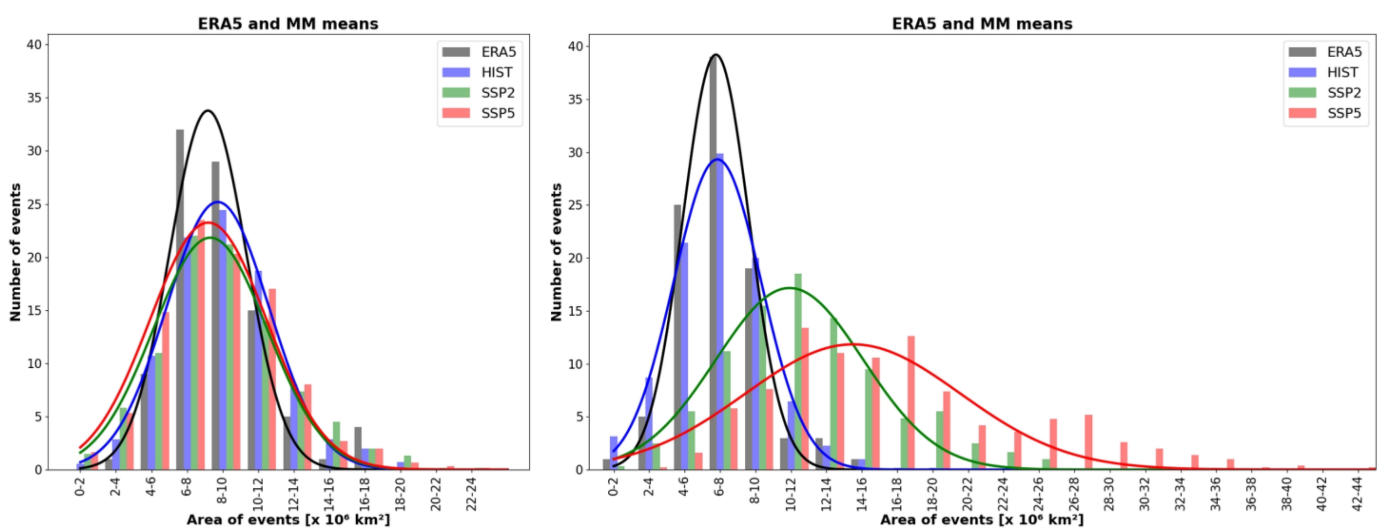

Figure 8. Occurrence of blocking events as a function of area for ERA5 and the GCMs during HIST, SSP2, and SSP5 considering $\Delta Z500_{HIST}$, $\Delta Z500_{SSP2}$, and $\Delta Z500_{SSP5}$ (*left*) and $\Delta Z500$~~$_{SSP}$~~$_{SSP2\text{-}HIST}$ and $\Delta Z500_{SSP5\text{-}HIST}$ (*right*). Gaussian fits are drawn for ERA5 and MM means. (GFDL is excluded from the MM means of ~~SSP5 in~~ $\Delta Z500$~~$_{HIST}$~~$_{SSP5\text{-}HIST}$.)

~~Mean area of blocking events computed with the DG method versus mean area of blocking events computed with the center method considering $\Delta Z500_{\mathrm{HIST}}$ *(left)* and $\Delta Z500_{\mathrm{SSP}}$ *(right)*. R is the correlation; R^* is the correlation excluding GFDL; a is the slope of the linear regression; regression lines (found by the least-squares fit excluding GFDL in SSP5 in *(left)*) are drawn when the correlation is statistically significant (at the 95% confidence level).~~

5 Conclusions

We identify wintertime European blocking events by applying the weather type decomposition methodology on the European-Atlantic sector. Our aim is to quantify the impact of climate change on the frequency, duration, and ~~extension~~ size of blocking events. For this purpose, we consider 30 years of historical runs and two future scenarios (SSP2-4.5 and SSP5-8.5) of nine CMIP6-GCMs. We show that the GCMs considered in this study capture well the spatio-temporal characteristics of atmospheric blocking, nevertheless, only those representing blocking patterns and variability closer to the reanalysis are used to investigate future blocking changes.

~~Considering two types of geopotential anomalies, which use a different climatology as a reference ($\Delta Z500_{\mathrm{HIST}}$ and $\Delta Z500_{\mathrm{SSP}}$), we can attribute the future changes of blocking to the total signal or to the dynamical signal of climate change.~~ We find that the impact of climate change on blocking frequency and duration is not statistically significant, consistent with the literature ~~results~~ that there is no general consensus on the tendency of blocking ~~event~~ frequency in the future (Woollings et al., 2018). ~~The fact that the results obtained for blocking event frequency and duration with $\Delta Z500_{\mathrm{HIST}}$ are similar to the ones obtained with $\Delta Z500_{\mathrm{SSP}}$ suggests that changes in temporal characteristics of blocking are not only influenced by the global warming of the 21st century but also by changes in regional circulation.~~

~~We define a new methodology, the center method ,~~ We introduce the composite method to quantify the ~~extension of blocking events~~size of blocking composites. We find that blocking area and center intensity are linearly correlated. ~~We apply another method, the DG method, and obtain similar results. This implies that the area of a blocking event can be computed indifferently either by the WTD for the center method or by the DG index for the DG method.~~

~~Climate change will significantly increase the extension of blocking events in the future especially in the worst-case scenario.~~ Blocking patterns and ~~extension obtained with $\Delta Z500_{\mathrm{SSP}}$~~ size in the future are similar to the results obtained for the recent-past climate. This means that the spatial characteristics of blocking events will not change at the end of the century with respect to the ~~climatology of the considered 30-year period and that the blocking extension increase due to climate change is mainly due to higher~~ future atmospheric mean state. Instead, if we take into account the increasing geopotential height caused by ~~warmer climate~~a warmer climate, we find that the size of blocking events will significantly increase in the future, especially in the worst-case scenario. ~~Similar considerations are also valid for the mean intensities of the blocking centers: they will increase during SSP2 and even more during SSP5 with respect to the recent-past conditions (using $\Delta Z500_{\mathrm{HIST}}$) because of the thermodynamical signal of climate change.~~

We also apply another method, the DG method, to compute the blocking size, and we obtain similar results.

In general, we observe that the differences between SSP2- and SSP5-results are smaller than differences among the various GCM-results, suggesting that there is no clear signal of climate change on blocking frequency, duration, and size. To the best of our knowledge, this is the first study investigating ~~frequency, duration, and extension~~ these characteristics of blocking events that are identified via the WTD. Moreover, there are still few studies addressing this topic using GCMs of the CMIP6. Our results are in agreement with previous findings where blocking events are defined with blocking indexes. This confirms that the application of the WTD is also a good strategy to analyse blocking event characteristics.

This study could be improved by analysing more GCMs, although other studies that considered many GCMs initially used only the best few GCMs for the analysis later; for example, Lee and Ahn (2017) selected five GCMs among twenty-two CMIP5-GCMs to study atmospheric blocking over the Pacific Ocean. Before comparing blocking event areas with other studies, it must be reminded that the results depend on the defined threshold. Finally, it must pointed out that the four weather types imposed in the k-means algorithm allow to recover the ones usually obtained with the reanalysis. However, a different number of weather types may need to be computed in some models where the variability is different from the reanalysis (e.g. five regimes are considered in the CNRM model by Ménégoz et al. (2018)).

Author contributions. All authors contributed to designing the study. SB and FJ analysed the data, together with ELB, and produced the figures. All the authors discussed the results. SB wrote the paper; all the authors provided assistance in finalizing the article.

Competing interests. The authors declare that they have no conflict of interest.

Acknowledgements. The authors thank Dr. E. Nabizadeh and Prof. P. Hassanzadeh for the useful discussion. The authors acknowledge the World Climate Research Programme (WCRP), which coordinated and promoted CMIP6, the climate modeling groups for producing and making available their model output, and the Mésocentre ESPRI (Ensemble de services pour la recherche à l'IPSL, https://mesocentre.ipsl.fr/) for archiving the data and providing the access to the CMIP6 data. SB thanks the LEGI for the postdoctoral support; ELB and FJ thank the IDEX program MobilAir for the PhD and MSc support, respectively.

References

Barnes, E. A., Dunn-Sigouin, E., Masato, G., and Woollings, T.: Exploring recent trends in Northern Hemisphere blocking, Geophysical Research Letters, 41, 638–644, https://doi.org/10.1002/2013GL058745, 2014.

Barriopedro, D., García-Herrera, R., Lupo, A. R., and Hernández, E.: A Climatology of Northern Hemisphere Blocking, Journal of Climate, 19, 1042–1063, https://doi.org/10.1175/JCLI3678.1, 2006.

Barriopedro, D., García-Herrera, R., and Trigo, R. M.: Application of blocking diagnosis methods to General Circulation Models. Part I: a novel detection scheme, Climate Dynamics, 35, 1373–1391, https://doi.org/10.1007/s00382-010-0767-5, 2010.

Berckmans, J., Woollings, T., Demory, M.-E., Vidale, P.-L., and Roberts, M.: Atmospheric blocking in a high resolution climate model: influences of mean state, orography and eddy forcing, Atmospheric Science Letters, 14, 34–40, https://doi.org/10.1002/asl2.412, 2013.

Boé, J. and Terray, L.: A Weather-Type Approach to Analyzing Winter Precipitation in France: Twentieth-Century Trends and the Role of Anthropogenic Forcing, Journal of Climate, 21, 3118–3133, https://doi.org/10.1175/2007JCLI1796.1, 2008.

Cassou, C.: Intraseasonal interaction between the Madden–Julian Oscillation and the North Atlantic Oscillation, Nature, 455, 523–527, https://doi.org/10.1038/nature07286, 2008.

Cassou, C., Terray, L., Hurrell, J. W., and Deser, C.: North Atlantic Winter Climate Regimes: Spatial Asymmetry, Stationarity with Time, and Oceanic Forcing, Journal of Climate, 17, 1055–1068, https://doi.org/10.1175/1520-0442(2004)017<1055:NAWCRS>2.0.CO;2, 2004.

Cassou, C., Terray, L., and Phillips, A.: Tropical Atlantic Influence on European Heat Waves, Journal of Climate, 18, 2805–2811, https://doi.org/10.1175/JCLI3506.1, 2005.

Cattiaux, J., Douville, H., and Peings, Y.: European temperatures in CMIP5: origins of present-day biases and future uncertainties, Clim Dyn, 41, 2889–2907, https://doi.org/10.1007/s00382-013-1731-y, 2013.

Cheung, H., Zhou, W., Mok, H., Wu, M., and Shao, Y.: Revisiting the climatology of atmospheric blocking in the Northern Hemisphere, Adv. Atmos. Sci., 30, 397–410, https://doi.org/10.1007/s00376-012-2006-y, 2013.

Chhin, R. and Yoden, S.: Ranking CMIP5 GCMs for Model Ensemble Selection on Regional Scale: Case Study of the Indochina Region, Journal of Geophysical Research: Atmospheres, 123, 8949–8974, https://doi.org/10.1029/2017JD028026, 2018.

Chung, C. and Nigam, S.: Weighting of geophysical data in Principal Component Analysis, Journal of Geophysical Research: Atmospheres, 104, 16 925–16 928, https://doi.org/10.1029/1999JD900234, 1999.

Cortesi, N., Torralba, V., Gonzáez-Reviriego, N., Soret, A., and J.Doblas-Reyes, F.: Characterization of European wind speed variability using weather regimes, Climate Dynamics, 53, 4961–4976, https://doi.org/10.1007/s00382-019-04839-5, 2019.

Davini, D. and D'Andrea, F.: From CMIP3 to CMIP6: Northern Hemisphere Atmospheric Blocking Simulation in Present and Future Climate, Journal of Climate, 33, 10 021–10 038, https://doi.org/10.1175/JCLI-D-19-0862.1, 2020.

Davini, P., Cagnazzo, C., and Anstey, J. A.: A blocking view of the stratosphere-troposphere coupling, Journal of Geophysical Research: Atmospheres, 119, 11,100–11,115, https://doi.org/10.1002/2014JD021703, 2014.

Davini, P., Corti, S., D'Andrea, F., Rivière, G., and von Hardenberg, J.: Improved Winter European Atmospheric Blocking Frequencies in High-Resolution Global Climate Simulations, Journal of Advances in Modeling Earth Systems, 9, 2615–2634, https://doi.org/10.1002/2017MS001082, 2017.

Dole, R. M. and Gordon, N. D.: Persistent Anomalies of the Extratropical Northern Hemisphere Wintertime Circulation: Geographical Distribution and Regional Persistence Characteristics, Monthly Weather Review, 111, 1567–1586, https://doi.org/10.1175/1520-0493(1983)111<1567:PAOTEN>2.0.CO;2, 1983.

Drouard, M. and Woollings, T.: Contrasting Mechanisms of Summer Blocking Over Western Eurasia, Geophysical Research Letters, 45, 12,040–12,048, https://doi.org/10.1029/2018GL079894, 2018.

Dunn-Sigouin, E. and Son, S.-W.: Northern Hemisphere blocking frequency and duration in the CMIP5 models, Journal of Geophysical Research: Atmospheres, 118, 1179–1188, https://doi.org/10.1002/jgrd.50143, 2013.

Dunn-Sigouin, E., Son, S.-W., and Lin, H.: Evaluation of Northern Hemisphere Blocking Climatology in the Global Environment Multiscale Model, Monthly Weather Review, 141, 707–727, https://doi.org/10.1175/MWR-D-12-00134.1, 2013.

Eyring, V., Bony, S., Meehl, G. A., Senior, C. A., Stevens, B., Stouffer, R. J., and Taylor, K. E.: Overview of the Coupled Model Intercomparison Project Phase 6 (CMIP6) experimental design and organization, Geoscientific Model Development, 9, 1937–1958, https://doi.org/10.5194/gmd-9-1937-2016, 2016.

Fabiano, F., Meccia, V., Davini, P., Ghinassi, P., and Corti, S.: A regime view of future atmospheric circulation changes in Northern midlatitudes, Weather and Climate Dynamics Discussions, 2020, 1–24, https://doi.org/10.5194/wcd-2020-37, 2020.

Hassanzadeh, P., Kuang, Z., and Farrell, B. F.: Responses of midlatitude blocks and wave amplitude to changes in the meridional temperature gradient in an idealized dry GCM, Geophysical Research Letters, 41, 5223–5232, https://doi.org/10.1002/2014GL060764, 2014.

Hausfather, Z. and Peters, G.: Emissions – the 'businessas usual' story is misleading, Nature, 577, 618–620, https://doi.org/10.1038/d41586-020-00177-3, 2020.

Hersbach, H., Bell, B., Berrisford, P., Hirahara, S., Horányi, A., Muñoz Sabater, J., Nicolas, J., Peubey, C., Radu, R., Schepers, D., Simmons, A., Soci, C., Abdalla, S., Abellan, X., Balsamo, G., Bechtold, P., Biavati, G., Bidlot, J., Bonavita, M., De Chiara, G., Dahlgren, P., Dee, D., Diamantakis, M., Dragani, R., Flemming, J., Forbes, R., Fuentes, M., Geer, A., Haimberger, L., Healy, S., Hogan, R. J., Hólm, E., Janisková, M., Keeley, S., Laloyaux, P., Lopez, P., Lupu, C., Radnoti, G., de Rosnay, P., Rozum, I., Vamborg, F., Villaume, S., and Thépaut, J.-N.: The ERA5 global reanalysis, Quarterly Journal of the Royal Meteorological Society, 146, 1999–2049, https://doi.org/10.1002/qj.3803, 2020.

Hertig, E. and Jacobeit, J.: Variability of weather regimes in the North Atlantic-European area: past and future, Atmospheric Science Letters, 15, 314–320, https://doi.org/10.1002/asl2.505, 2014.

Hou, P. and Wu, S.: Long-term Changes in Extreme Air Pollution Meteorology and the Implications for Air Quality, Scientific Reports, 6, 23 792, https://doi.org/10.1038/srep23792, 2016.

Jiménez, P. A., González-Rouco, J., Montávez, J., García-Bustamante, E., and Navarro, J.: Climatology of wind patterns in the northeast of the Iberian Peninsula, International Journal of Climatology, 29, 501–525, https://doi.org/10.1002/joc.1705, 2009.

Khan, N., Shahid, S., Ahmed, K., Wang, X., Ali, R., Ismail, T., and Nawaz, N.: Selection of GCMs for the projection of spatial distribution of heat waves in Pakistan, Atmospheric Research, 233, 104 688, https://doi.org/10.1016/j.atmosres.2019.104688, 2020.

Largeron, Y. and Staquet, C.: Persistent inversion dynamics and wintertime PM_{10} air pollution in Alpine valleys, Atmospheric Environment, 135, 92–108, https://doi.org/10.1016/j.atmosenv.2016.03.045, 2016.

Lee, D. Y. and Ahn, J.-B.: Future change in the frequency and intensity of wintertime North Pacific blocking in CMIP5 models, International Journal of Climatology, 37, 2765–2781, https://doi.org/10.1002/joc.4878, 2017.

Lupo, A., Jensen, A., Mokhov, I., Timazhev, A., Eichler, T., and Efe, B.: Changes in Global Blocking Character in Recent Decades, Atmosphere, 10, https://doi.org/10.3390/atmos10020092, 2019.

Masato, G., Hoskins, B. J., and Woollings, T.: Winter and Summer Northern Hemisphere Blocking in CMIP5 Models, Journal of Climate, 26, 7044–7059, https://doi.org/10.1175/JCLI-D-12-00466.1, 2013.

Masato, G., Woollings, T., and Hoskins, B. J.: Structure and impact of atmospheric blocking over the Euro-Atlantic region in present-day and future simulations, Geophysical Research Letters, 41, 1051–1058, https://doi.org/10.1002/2013GL058570, 2014.

Matsueda, M. and Endo, H.: The robustness of future changes in Northern Hemisphere blocking: A large ensemble projection with multiple sea surface temperature patterns, Geophysical Research Letters, 44, 5158–5166, https://doi.org/10.1002/2017GL073336, 2017.

Matsueda, M., Mizuta, R., and Kusunoki, S.: Future change in wintertime atmospheric blocking simulated using a 20-km-mesh atmospheric global circulation model, Journal of Geophysical Research: Atmospheres, 114, https://doi.org/10.1029/2009JD011919, 2009.

Ménégoz, M., Cassou, C., Swingedouw, D., Ruprich-Robert, Y., Bretonniére, P.-A., and Doblas-Reyes, D.: Role of the Atlantic Multidecadal Variability in modulating the climate response to a Pinatubo-like volcanic eruption, Climate Dynamics, 51, 1863–1883, https://doi.org/10.1007/s00382-017-3986-1, 2018.

Michelangeli, P.-A., Vautard, R., and Legras, B.: Weather Regimes: Recurrence and Quasi Stationarity, Journal of the Atmospheric Sciences, 52, 1237–1256, https://doi.org/10.1175/1520-0469(1995)052<1237:WRRAQS>2.0.CO;2, 1995.

Mokhov, I. and Timazhev, A.: Atmospheric Blocking and Changes in its Frequency in the 21st Century Simulated with the Ensemble of Climate Models, Russ. Meteorol. Hydrol, pp. 369–377, https://doi.org/10.3103/S1068373919060013, 2019.

Mokhov, I., Akperov, M., Prokofyeva, M., Timazhev, A., Lupo, A., and Le Treut, H.: Blockings in the Northern Hemisphere and EuroAtlantic Region:Estimates of Changes from Reanalysis Data and Model Simulations, Doklady Earth Sciences, 449, 430–433, https://doi.org/10.1134/S1028334X13040144, 2013.

Mokhov, I. I., Timazhev, A. V., and Lupo, A. R.: Changes in atmospheric blocking characteristics within Euro-Atlantic region and Northern Hemisphere as a whole in the 21st century from model simulations using RCP anthropogenic scenarios, Global and Planetary Change, 122, 265–270, https://doi.org/10.1016/j.gloplacha.2014.09.004, 2014.

Munoz, C., Schultz, D., and Vaughan, G.: A Midlatitude Climatology and Interannual Variability of 200- and 500-hPa Cut-Off Lows, Journal of Climate, 33, 2201–2222, https://doi.org/10.1175/JCLI-D-19-0497.1, 2020.

Nabizadeh, E., Hassanzadeh, P., Yang, D., and Barnes, E. A.: Size of the Atmospheric Blocking Events: Scaling Law and Response to Climate Change, Geophysical Research Letters, 46, 13 488–13 499, https://doi.org/10.1029/2019GL084863, 2019.

Patterson, M., Bracegirdle, T., and Woollings, T.: Southern Hemisphere Atmospheric Blocking in CMIP5 and Future Changes in the Australia-New Zealand Sector, Geophysical Research Letters, 46, 9281–9290, https://doi.org/10.1029/2019GL083264, 2019.

Philipp, A., Beck, C., Huth, R., and Jacobeit, J.: Development and comparison of circulation type classifications using the COST 733 dataset and software, International Journal of Climatology, 36, 2673–2691, https://doi.org/10.1002/joc.3920, 2016.

Pinheiro, M., Ullrich, P., and Grotjahn, R.: Atmospheric blocking and intercomparison of objective detection methods: flow field characteristics, Climate Dynamics, 53, 4189–4216, https://doi.org/10.1007/s00382-019-04782-5, 2019.

Riahi, K., van Vuuren, D. P., Kriegler, E., Edmonds, J., O'Neill, B. C., Fujimori, S., Bauer, N., Calvin, K., Dellink, R., Fricko, O., Lutz, W., Popp, A., Cuaresma, J. C., KC, S., Leimbach, M., Jiang, L., Kram, T., Rao, S., Emmerling, J., Ebi, K., Hasegawa, T., Havlik, P., Humpenöder, F., Da Silva, L. A., Smith, S., Stehfest, E., Bosetti, V., Eom, J., Gernaat, D., Masui, T., Rogelj, J., Strefler, J., Drouet, L., Krey, V., Luderer, G., Harmsen, M., Takahashi, K., Baumstark, L., Doelman, J. C., Kainuma, M., Klimont, Z., Marangoni, G., Lotze-Campen, H., Obersteiner, M., Tabeau, A., and Tavoni, M.: The Shared Socioeconomic Pathways and their energy, land use, and greenhouse gas emissions implications: An overview, Global Environmental Change, 42, 153–168, https://doi.org/10.1016/j.gloenvcha.2016.05.009, 2017.

Russo, A., Trigo, R. M., Martins, H., and Mendes, M. T.: NO2, PM10 and O3 urban concentrations and its association with circulation weather types in Portugal, Atmospheric Environment, 89, 768–785, https://doi.org/10.1016/j.atmosenv.2014.02.010, 2014.

Sáenz, F. and Durán-Quesada, A.: A climatology of low level windregimes over Central America using aweather type classification approach, Front. Earth Sci., 3, https://doi.org/10.3389/feart.2015.00015, 2015.

Schiemann, R., Demory, M., Shaffrey, L. C., Strachan, J., Vidale, P. L., Mizielinski, M. S., Roberts, M. J., Matsueda, M., Wehner, M. F., and Jung, T.: The Resolution Sensitivity of Northern Hemisphere Blocking in Four 25-km Atmospheric Global Circulation Models, Journal of Climate, 30, 337–358, https://doi.org/10.1175/JCLI-D-16-0100.1, 2017.

Sillmann, J. and Croci-Maspoli, M.: Present and future atmospheric blocking and its impact on European mean and extreme climate, Geophysical Research Letters, 36, https://doi.org/10.1029/2009GL038259, 2009.

Tibaldi, S. and Molteni, F.: On the operational predictability of blocking, Tellus A, 42, 343–365, https://doi.org/10.1034/j.1600-0870.1990.t01-2-00003.x, 1990.

Ullmann, A., Fontaine, B., and Roucou, P.: Euro-Atlantic weather regimes and Mediterranean rainfall patterns: present-day variability and expected changes under CMIP5 projections, International Journal of Climatology, 34, 2634–2650, https://doi.org/10.1002/joc.3864, 2014.

Whiteman, C. D.: Breakup of Temperature Inversions in Deep Mountain Valleys: Part I. Observations, Journal of Applied Meteorology, 21, 270–289, https://doi.org/10.1175/1520-0450(1982)021<0270:BOTIID>2.0.CO;2, 1982.

Wiedenmann, J. M., Lupo, A. R., Mokhov, I. I., and Tikhonova, E. A.: The Climatology of Blocking Anticyclones for the Northern and Southern Hemispheres: Block Intensity as a Diagnostic, Journal of Climate, 15, 3459–3473, https://doi.org/10.1175/1520-0442(2002)015<3459:TCOBAF>2.0.CO;2, 2002.

Woollings, T., Barriopedro, D., Methven, J., Son, S.-W., Martius, O., Harvey, B., Sillmann, J., Lupo, A. R., and Seneviratne, S.: Blocking and its Response to Climate Change, Current Climate Change Reports, 4, 287–300, https://doi.org/10.1007/s40641-018-0108-z, 2018.